Stability Tool for Electric Power Systems with a High Penetration of Electronic Power Converters

D. Serrano-Jiménez[1], E. Unamuno[1*], A. Gil de Muro[2], D. A. Aragón-Sotelo[2], S. Ceballos[2], J. A. Barrena[1]

[1]*Electronics and Computing Department, Mondragon Unibertsitatea, Loramendi 4, 20500 Mondragon, Spain*
[2]*Tecnalia, Basque Research and Technology Alliance (BRTA), Parque Tecnológico de Bizkaia, 48160 Derio, Spain*
[*] *Corresponding author (eunamuno@mondragon.edu)*

Abstract

The increasing use of electronic converters is making possible the development of more sustainable, efficient, and reliable electric power systems, but it is also introducing new challenges that need to be addressed. Power system stability is one of them since the converter multiscale coupling between control loops and the mutual effects of multiple converters make the traditional approaches and specialized software available not fully adequate. In this context, this paper presents a software tool called CSTEP capable of carrying out small- and large-signal stability analysis for electric power systems strongly dominated by electronic converters. By utilizing the tool description, the paper provides the reader with a systematic methodology to obtain the system dynamic representation, and with some software tools for the analysis of the large and small-signal stability. Finally, the validity and functionality of CSTEP have tested with the implementation of three use cases: a simple ac use case to illustrate the application of the system algorithm step by step, an IEEE 5-bus use case to validate the tool with already established commercial software and a more realistic system based on a medium voltage CIGRÉ benchmark to highlight the potential applications of the tool. The results show that, unlike existing tools that simplify or neglect the electric part of the grid (filters, line impedances, etc.), CSTEP can predict power system instabilities caused by the interactions of fast control loops of electronic converters with the electric part.

Keywords: converter stability, electric power system, electronic converters, modal analysis, power system modelling, power system simulation, power system stability, small-signal analysis

Nomenclature

Indices	
i	Element number
j	Eigenvalue number
k	Parameter number
l	State number

Sets	
E	Element
S	System

Subscripts	
int	Internal
pn	Potential node
fn	Flow node
ip	Input port
op	Output port

Variables	
$\mathbf{x}$	Differential (state) variables
$\mathbf{z}$	Algebraic variables
$\mathbf{u}$	External input variables
$\mathbf{np}$	System node potential variables
$\mathbf{pp}$	System port potential variables
$\mathbf{A}$	State matrix
$\mathbf{B}$	Input matrix
λ	System eigenvalue
$\mathbf{\Phi}$	Left eigenvector of state matrix $\mathbf{A}$
$\mathbf{\Psi}$	Right eigenvector of state matrix $\mathbf{A}$
$\mathbf{pf}$	Participation factors
$\mathbf{wpf}$	Weighted participation factors
$\mathbf{ps}$	Parametric sensitivities
$\mathbf{rps}$	Real part of parametric sensitivities
ρ	System parameter

1. Introduction

Electric power systems are undergoing an unprecedented transformation motivated by the need of increasing their sustainability, efficiency, and reliability. The introduction of electronic converters is helping enormously in this regard, but it is also introducing new challenges that need to be addressed [1]. Among them, power system stability is one of the most important to consider. Power system stability is defined as the ability of an electrical system, for a given initial condition, to regain a state of operating equilibrium after being subjected to a disturbance, with most system variables bounded [2]. Traditionally, the assessment of the stability has been divided into angle, frequency, and voltage, further divided into small- and large-signal analyses depending on the magnitude of the disturbance studied [2].

This division is based on a time-scale separation of the electromechanical oscillations associated with synchronous generators and the electromagnetic oscillations related to the electrical part of the grid. With the massive integration of electronic power converters and their controls, the previous assumption is no longer valid for all power systems [3]. Converters can be controlled to mimic the behaviour of classical synchronous machines but with a much faster response to ensure the stability of the power system [4].

Therefore, the converter multiscale coupling between control loops and the mutual interactions of parallel converters frequently requires the consideration of the electromagnetic as well as the electromechanical dynamics [5]. In light of this issue, an extended classification has been recently presented incorporating the term *converter-driven stability* to consider this type of coupling in the assessment of stability [6]. Converter-driven or converter stability can be divided into small-signal and large-signal analyses [7]. In small-signal studies, the system is linearized around an operation point and thus, the conclusions drawn are valid for small deviations from this operation point. The advantage of small-signal studies is that, since the system is linear, all the powerful linear analysis tools can be applied. Such studies can be divided into time-domain or frequency-domain, depending on the type of system representation employed [8].

Time-domain studies are carried out with state-space representations, by looking at the location of eigenvalues in the complex plane and their properties (damping factor, natural frequency, oscillation frequency, etc.). Recently, the so-called component connection method (CCM) has been proposed to facilitate the construction of systems comprised of several devices (generators, loads, converters, etc.) [9]. One of the main disadvantages of this method and similar ones is that it does not reduce these redundant states and therefore the models of devices must be modified depending on how they are connected (e.g., when connecting two nominal-pi equivalent transmission line models, the state representing the voltage at one of the terminal capacitors is redundant).

Frequency-domain studies are based on impedance-based representations, which enable the construction of power systems by means of equivalent voltage/current sources and impedances [10]. The advantages of such representations are

that small-signal stability margins can be quantified, and their modularity and scalability are high. Moreover, a black-box model can be obtained using a frequency-scanning method [8].

Even though there are tools such as MATLAB that provide commands or libraries to facilitate the construction of small-signal time- and frequency-domain models for the assessment of the converter stability, to the best of the authors' knowledge, there are no standardized tools to carry out such studies systematically. Each model must be constructed ad hoc, defining the equations of all the devices connected to the system under study. This means that if a device appears more than once in the system (e.g., the *RL* impedance of a line), its model cannot be reutilized and the equations have to be repeated in the overall model, but modifying the variable names. Moreover, all studies focus either on time- or frequency-domain representations but do not take full advantage of combining both approaches.

Regarding large-signal stability analysis, two main methods can be distinguished: Lyapunov-based techniques and time-domain simulations. Considering the difficulty in generalizing a method based on Lyapunov, time-domain simulations are the default solution for studying the large-signal stability of any power system scenario. As it was previously explained, in conventional power systems dominated by synchronous generators electromagnetic transients (EMT) are neglected, and RMS or quasi-steady-state (QSS) phasor simulations are used to increase the computational speed [11].

The available tools that consider EMT dynamics mainly focus on the analysis of transient values of voltages and currents for element sizing and design purposes [12], rather than on large-signal stability analyses. More general-purpose tools such as MATLAB require the development of ad hoc models of the system to be analysed [13]. The former do not provide information about the modes or eigenvalues associated with the electrical part of the system for the assessment of the small-signal stability, and the latter are usually focused on the analysis and design of controllers for electronic converters rather than on the overall analysis of the power system [4,14–16]. Other co-simulation tools that combine electromechanical and electromagnetic dynamics have been also developed to simulate power systems with a high presence of electronic power converters in the time domain [17,18]. These tools are usually oriented to system planning but do not return the root loci of the system to carry out small-signal stability analyses.

In this paper, a MATLAB-based software tool called CSTEP (Converter Stability Tool for Electric Power Systems) is presented to construct and analyse the small- and large-signal stability of converter-dominated power systems. The mathematical foundations of the tool are similar to other tools focused for instance on EMT simulations of electrical and electronic circuits [19]. However, CSTEP incorporates a systematic formulation of state-space representations that, in addition to time-domain simulations, is aimed at small-signal stability studies by providing the root loci of the system under study. The dynamical models of the elements that comprise the test case are modelled in a library so that they can be used multiple times with different parameters. This facilitates the construction of complex systems without the need to repeat and

interconnect all the equations of the individual elements. Therefore, an important contribution of CSTEP is found in its element-oriented modelling philosophy, which makes it a modular and flexible tool. A difference with other tools is the capacity of CSTEP to automatically eliminate dependent dynamic states, which is necessary to handle applications such as synchronous generators or power converters with *L* or *LCL* filters connected to inductive lines or transformers, or power distribution systems with meshed or ring topologies where the currents are dependent on each other.

Another advantage of CSTEP compared to already existing software is its symbolic engine—in addition to the numerical one—enabling the generation of parametric state-space models that can be studied analytically and evaluated iteratively e.g., to determine the influence of parameters on the stability margins of the system. Moreover, unlike other simulation tools, the symbolic engine provides the analytical expressions that represent the dynamics of the system, which is interesting to identify the variables and parameters that determine the evolution of the states in the time domain.

Moreover, CSTEP includes a simulation module capable of assessing the time-domain behaviour of the constructed system by simulating the original set of nonlinear equations. These simulations provide information about the large-signal stability of the system and facilitate the validation of small-signal models before the analysis phase without the necessity to reconstruct the system in another tool.

The main objective of the paper is to provide the readers with the mathematical foundations and the methodology behind CSTEP for carrying out stability analyses of converter-dominated power systems. In Section 2, the main functions or modules to construct and analyse such systems are comprehensively described, and the potential extensions of the tool are highlighted. In Section 3, the use of CSTEP is illustrated by means of three use cases; the first demonstrates how a system is built in CSTEP with the proposed methodology, the second validates the large-signal results compared to a commercial tool and exhibits the problems that might arise when electromagnetic states are not considered in converter stability studies, and the third shows some of the potential applications that could be studied with the tool in a more complex case. Finally, in the last section, the main conclusions of the paper are gathered.

2. Description of CSTEP

The general structure of CSTEP is illustrated in Figure 1.

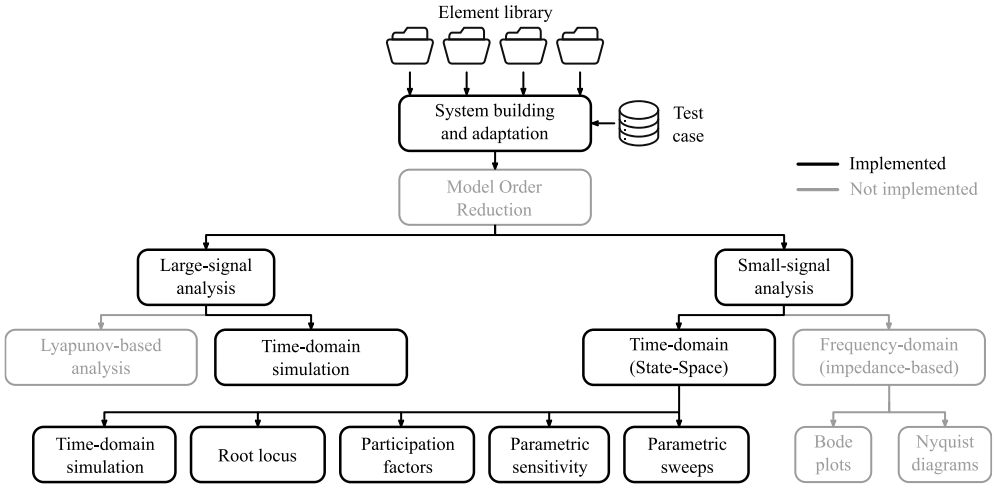

Figure 1 – CSTEP general structure

In the following sections, each of the core modules of CSTEP is described in detail. The modular nature of the tool will facilitate the integration of new modules to manipulate and broaden the study of the system equations in the future. For instance, it might be interesting to implement model order reduction (MOR) techniques to decouple states with different dynamics and to focus the subsequent analyses on the dynamics of interest [20]. The reader should not confuse MOR techniques with the reduction of redundant states mentioned in the following sections. Another interesting feature would be the implementation of a semiautomatic frequency-domain analysis tool to complement the information obtained from time-domain studies as in [21]. The core modules of CSTEP could be also extended to handle multi-harmonic models based on dynamic phasors or harmonic state-space systems [8,22]. These functionalities have been represented in grey in Figure 1.

A. System-building and adaptation module

The objective of the system-building and adaptation module is the definition of the system equations and the automatic construction, reduction and linearization of the model. Since CSTEP is an element-oriented tool, the equations of the system to be modelled are obtained by means of the equations of the individual elements and their interconnections. This means that first, it is necessary to define appropriate element representations. Based on these individual models and their interconnections (predefined in a test case file), the complete system is then constructed, reduced, and (if necessary) linearized at a specific operating point.

1) Element representation

CSTEP uses three different types of variables for the element representation: *internal*, *nodal*, and *port*. The internal variables are used to describe the intrinsic behaviour of the element and they can be differential ($\mathbf{x}_{int}$) or algebraic ($\mathbf{z}_{int}$). On the other hand, the nodal and port variables are used to define the connections between the elements and are always algebraic. Nodes refer to the connections used to transmit power, while ports refer to the connections used to transmit

information (e.g., control signals). Each node has two associated variables, i.e., a potential variable ($\mathbf{z}_{pn}$) and a flow variable ($\mathbf{z}_{fn}$). In power systems, potential and flow variables are associated with voltages and currents, respectively. In other domains, an analogous representation can be made, e.g.: speed and torque in mechanical systems; temperature and heat flow in thermal circuits, or the magnetic field and flux in magnetic circuits. The formulation of CSTEP described in the following sections is kept generic so that various domains can be combined in the future. Port variables are divided into input variables ($\mathbf{z}_{ip}$) and output variables ($\mathbf{z}_{op}$).

Considering all this information, the number of equations required for the representation of an element must be equal to the number of equations of internal differential variables ($\mathbf{f}$), plus the number of equations of internal algebraic variables ($\mathbf{g}_1$) plus the number of equations of node variables ($\mathbf{g}_2$), plus the number of equations of output port variables ($\mathbf{g}_3$). These equations are shown in the following expressions:

$$\dot{\mathbf{x}}_{int}^{E_i} = \mathbf{f}^{E_i}\left(\mathbf{x}_{int}^{E_i}, \mathbf{z}_{int}^{E_i}, \mathbf{z}_{pn}^{E_i}, \mathbf{z}_{fn}^{E_i}, \mathbf{z}_{ip}^{E_i}, \mathbf{z}_{op}^{E_i}, \mathbf{u}^{E_i}\right) \tag{1}$$

$$\mathbf{0} = \mathbf{g}_1^{E_i}\left(\mathbf{x}_{int}^{E_i}, \mathbf{z}_{int}^{E_i}, \mathbf{z}_{pn}^{E_i}, \mathbf{z}_{fn}^{E_i}, \mathbf{z}_{ip}^{E_i}, \mathbf{z}_{op}^{E_i}, \mathbf{u}^{E_i}\right) \tag{2}$$

$$\mathbf{0} = \mathbf{g}_2^{E_i}\left(\mathbf{x}_{int}^{E_i}, \mathbf{z}_{int}^{E_i}, \mathbf{z}_{pn}^{E_i}, \mathbf{z}_{fn}^{E_i}, \mathbf{z}_{ip}^{E_i}, \mathbf{z}_{op}^{E_i}, \mathbf{u}^{E_i}\right) \tag{3}$$

$$\mathbf{0} = \mathbf{g}_3^{E_i}\left(\mathbf{x}_{int}^{E_i}, \mathbf{z}_{int}^{E_i}, \mathbf{z}_{pn}^{E_i}, \mathbf{z}_{fn}^{E_i}, \mathbf{z}_{ip}^{E_i}, \mathbf{z}_{op}^{E_i}, \mathbf{u}^{E_i}\right) \tag{4}$$

where the superscript E_i represents the *i*-th element.

2) Nonreduced system representation

As it was previously explained, the system representation is obtained by means of the system models and their interconnections. The first step is for CSTEP to generate the nonreduced system representation consisting of the concatenation of the equations of the elements. This process leads to equations $\mathbf{f}^S$, $\mathbf{g}_1^S$, $\mathbf{g}_2^S$, and $\mathbf{g}_3^S$ shown in Eqs. (5)–(8). These expressions have a greater number of variables than the number of equations. To complete the system of equations, the system node potential variables (**np**) and the system port potential variables (**pp**) are defined based on the node and port variables of the individual elements. With these new variables, the relation between the node potential, input port and output port variables for each element is defined, obtaining equations $\mathbf{g}_4^S$, $\mathbf{g}_5^S$, and $\mathbf{g}_6^S$ shown in expressions (9)–(12). The current flow on each node of the system is defined according to Kirchhoff's current law to obtain $\mathbf{g}_7^S$. Finally, an additional reference node potential (np_0) is included and set to zero as shown in Eq. (13). This equation defines a common reference voltage for all the nodes in the system, which will be necessary to solve the system of equations.

$$\dot{\mathbf{x}}^S = \mathbf{f}^S \Leftrightarrow \left[\mathbf{x}_{int}^{E_1},\ldots,\mathbf{x}_{int}^{E_n}\right] = \left[\mathbf{f}^{E_1},\ldots,\mathbf{f}^{E_n}\right] \tag{5}$$

$$\mathbf{0} = \mathbf{g}_1^S \Leftrightarrow \left[\mathbf{0}_{g_1}^{E_1},\ldots,\mathbf{0}_{g_1}^{E_n}\right] = \left[\mathbf{g}_1^{E_1},\ldots,\mathbf{g}_1^{E_n}\right] \tag{6}$$

$$\mathbf{0} = \mathbf{g}_2^S \Leftrightarrow \left[\mathbf{0}_{g_2}^{E_1},\ldots,\mathbf{0}_{g_2}^{E_n}\right] = \left[\mathbf{g}_2^{E_1},\ldots,\mathbf{g}_2^{E_n}\right] \tag{7}$$

$$\mathbf{0} = \mathbf{g}_3^S \Leftrightarrow \left[\mathbf{0}_{g_3}^{E_1},\ldots,\mathbf{0}_{g_3}^{E_n}\right] = \left[\mathbf{g}_3^{E_1},\ldots,\mathbf{g}_3^{E_n}\right] \tag{8}$$

$$\mathbf{0} = \mathbf{g}_4^S = \left[\mathbf{g}_4^{E_1}\left(\mathbf{z}_{pn}^{E_1},\mathbf{np}\right),\ldots,\mathbf{g}_4^{E_n}\left(\mathbf{z}_{pn}^{E_n},\mathbf{np}\right)\right] \tag{9}$$

$$\mathbf{0} = \mathbf{g}_5^S = \left[\mathbf{g}_5^{E_1}\left(\mathbf{z}_{ip}^{E_1},\mathbf{pp}\right),\ldots,\mathbf{g}_5^{E_n}\left(\mathbf{z}_{ip}^{E_n},\mathbf{pp}\right)\right] \tag{10}$$

$$\mathbf{0} = \mathbf{g}_6^S = \left[\mathbf{g}_5^{E_1}\left(\mathbf{z}_{po}^{E_1},\mathbf{pp}\right),\ldots,\mathbf{g}_5^{E_n}\left(\mathbf{z}_{po}^{E_n},\mathbf{pp}\right)\right] \tag{11}$$

$$\mathbf{0} = \mathbf{g}_7\left(\mathbf{z}_{fn}^{E_1},\ldots,\mathbf{z}_{fn}^{E_n}\right) \tag{12}$$

$$0 = np_0 \tag{13}$$

where the superscript *S* denotes system-level equations.

Expressions (5)–(13) describe the dynamic performance of the electric power system. It is called a nonreduced representation because the algebraic variables are still present in the equations. To provide a more compact fashion of these equations, algebraic variables of individual elements and node and port potential variables are grouped into $\mathbf{z}^S$ and Eqs. (6)–(13) are grouped into $\mathbf{g}^S$, leading to the following nonreduced system representation:

$$\begin{aligned}\dot{\mathbf{x}}^S &= \mathbf{f}^S\left(\mathbf{x}^S,\mathbf{z}^S,\mathbf{u}^S\right)\\ \mathbf{0} &= \mathbf{g}^S\left(\mathbf{x}^S,\mathbf{z}^S,\mathbf{u}^S\right)\end{aligned} \tag{14}$$

3) Reduced and linearized system representation

The nonreduced system representation may also contain redundant (linearly dependent) differential and algebraic equations [19]. Some typical examples where redundant variables appear are synchronous generators or electronic power converters with *L* or *LCL* filters connected in series to transformers or transmission lines, cutsets formed by inductors and/or current sources in closed loops (e.g. in meshed or ring power system topologies) [23] or the cascaded interconnection of π or *T* transmission line models. To systematically identify and reduce these redundancies, Eq. (14) is first represented in the matrix form as:

$$\begin{aligned}\dot{\mathbf{x}}^S &= \mathbf{E}\mathbf{x}^S + \mathbf{F}\mathbf{z}^S + \mathbf{G}\mathbf{u}^S\\ \mathbf{0} &= \mathbf{H}\mathbf{x}^S + \mathbf{K}\mathbf{z}^S + \mathbf{L}\mathbf{u}^S\end{aligned} \tag{15}$$

where the matrices are obtained by partially differentiating the equations in Eq. (14) with respect to state variables ($\mathbf{x}^S$), algebraic variables ($\mathbf{z}^S$) and inputs ($\mathbf{u}^S$):

$$\begin{aligned}\mathbf{E} &= \frac{\partial \mathbf{f}^S}{\partial \mathbf{x}^S} \quad \mathbf{F} = \frac{\partial \mathbf{f}^S}{\partial \mathbf{z}^S} \quad \mathbf{G} = \frac{\partial \mathbf{f}^S}{\partial \mathbf{u}^S}\\ \mathbf{H} &= \frac{\partial \mathbf{g}^S}{\partial \mathbf{x}^S} \quad \mathbf{K} = \frac{\partial \mathbf{g}^S}{\partial \mathbf{z}^S} \quad \mathbf{L} = \frac{\partial \mathbf{g}^S}{\partial \mathbf{u}^S}\end{aligned} \tag{16}$$

At this point, it is worth noting that, if the original system in Eq. (14) is nonlinear, obtaining the matrices by means of the partial derivatives as in Eq. (16) will linearize the equations. The mathematical explanation behind this linearization is based on the Taylor series expansion of Eq. (14), which is detailed in Appendix A. The linearization of the model is a necessary step to represent the equations in matrix form and to apply classical linear analysis techniques to perform a small-signal stability assessment. When equations are linearized, Eq. (15) becomes:

$$\begin{aligned} \Delta\dot{\mathbf{x}}^S &= \mathbf{E}\Delta\mathbf{x}^S + \mathbf{F}\Delta\mathbf{z}^S + \mathbf{G}\Delta\mathbf{u}^S \\ \mathbf{0} &= \mathbf{H}\Delta\mathbf{x}^S + \mathbf{K}\Delta\mathbf{z}^S + \mathbf{L}\Delta\mathbf{u}^S \end{aligned} \tag{17}$$

where Δ represents variations around the equilibrium point as explained in Appendix A. For the sake of generality, the symbol Δ is not included in the following equations.

When dynamical systems are represented by sinusoidal magnitudes, it is not possible to find a constant steady-state equilibrium point, and therefore CSTEP makes it possible to model these systems in a *dq* rotatory frame such that the sinusoidal variables become constant. The zero sequence could be also considered in the analyses, as long as the employed library models include the equations that represent this sequence. However, most of the studies related to the assessment of the small-signal stability of power systems consider symmetrical and balanced situations and average power converter models, where the zero sequence can be safely neglected. Since it is out of the scope of the paper, the assessment of the stability of power systems with zero sequence components or unbalances is left as a future research activity.

In the next step, the redundant states of the system are reduced and the dependencies between the variables are identified. The process consists of arranging the equations in (15) in a matrix form as follows:

$$\mathbf{U} = \left[\begin{array}{c|ccc} \mathbf{I} & \mathbf{F} & \mathbf{E} & \mathbf{G} \\ \hline \mathbf{0} & \mathbf{K} & \mathbf{H} & \mathbf{L} \end{array}\right] \tag{18}$$

A Gauss-Jordan elimination method is used and the matrix $\mathbf{U}$ is reduced to a row echelon form. The resulting matrix can be represented as:

$$\mathbf{U}_r = \left[\begin{array}{c|ccc} \mathbf{I}_r & \mathbf{F}_r & \mathbf{E}_r & \mathbf{G}_r \\ \hline \mathbf{0} & \mathbf{K}_r & \mathbf{H}_r & \mathbf{L}_r \end{array}\right] \tag{19}$$

where the subscript *r* represents the reduced form of the matrices. This matrix can be also rewritten as a differential and algebraic system of equations:

$$\begin{aligned} \dot{\mathbf{x}}_r^S &= \mathbf{E}_r\mathbf{x}_r^S + \mathbf{F}_r\mathbf{z}_r^S + \mathbf{G}_r\mathbf{u}^S \\ \mathbf{0} &= \mathbf{H}_r\mathbf{x}_r^S + \mathbf{K}_r\mathbf{z}_r^S + \mathbf{L}_r\mathbf{u}^S \end{aligned} \tag{20}$$

where $\mathbf{x}_r^S$ and $\mathbf{z}_r^S$ represent the reduced vector of states and algebraic variables, respectively.

CSTEP offers the possibility to carry out this process either numerically or symbolically. The former is faster and makes it possible to apply most classical analysis techniques, but unlike the symbolic approach, it is not capable of retaining all the

information to carry out a parametric sensitivity analysis (explained in Section III-C-3) or to identify the variables that determine the dynamic behaviour of the system.

4) Small-signal system representation

The last step in the system-building and adaptation module is to obtain the simplified small-signal representation of the system in the form:

$$\dot{\mathbf{x}}_r^S = \mathbf{A}\mathbf{x}_r^S + \mathbf{B}\mathbf{u}^S \tag{21}$$

For that purpose, the algebraic variables are first isolated from the algebraic equations in (20):

$$\mathbf{z}^S = -\mathbf{K}_r^{-1}\left(\mathbf{H}_r\mathbf{x}^S + \mathbf{L}_r\mathbf{u}^S\right) \tag{22}$$

Note that when obtaining the row echelon form $\mathbf{U}_r$ in Eq. (19), $\mathbf{K}_r$ becomes an upper-diagonal square matrix whose diagonal terms are different from zero, meaning that $\mathbf{K}_r$ will be invertible.

Then, the right-hand side of (22) is incorporated into the differential equations in (20) as:

$$\dot{\mathbf{x}}_r^S = \mathbf{E}_r\mathbf{x}_r^S - \mathbf{F}_r\mathbf{K}_r^{-1}\left(\mathbf{H}_r\mathbf{x}_r^S + \mathbf{L}_r\mathbf{u}^S\right) + \mathbf{G}_r\mathbf{u}^S \tag{23}$$

From Eq. (23), $\mathbf{A}$ and $\mathbf{B}$ can be calculated as:

$$\begin{aligned}\mathbf{A} &= \mathbf{E}_r - \mathbf{F}_r\mathbf{K}_r^{-1}\mathbf{H}_r \\ \mathbf{B} &= \mathbf{G}_r - \mathbf{F}_r\mathbf{K}_r^{-1}\mathbf{L}_r\end{aligned} \tag{24}$$

B. Large-signal analysis module

The large-signal module has two main objectives: the calculation of the time-domain response of the system and the validation of the small-signal state-space model when the system is nonlinear.

To perform the nonlinear simulation, the reduced system of equations in Eq. (14) is dynamically solved. For that purpose, the vector of input variables is defined as a time-dependent array—since the inputs vary during the simulation—and the *ode15i* solver provided by MATLAB is used to solve the system of equations.

C. Small-signal analysis module

The analysis module is used to carry out a small-signal stability analysis of the system from the time-domain representation of equations.

1) Time-domain simulation

To simulate the linearized system, the representation shown in Eq. (21) is solved via the *lsim* function from MATLAB. The results from this simulation are represented on top of the results from the large-signal analysis to corroborate the correctness of the linearized model.

2) Root locus

The small-signal stability analysis is based on the study of the location of the eigenvalues in the complex plane. If the real part of the eigenvalues is negative, the system is stable, and it will reach a new equilibrium point under a small disturbance. The tool returns the root locus of the system for the operation point provided by the user.

3) Participation factors

To analyse the system dynamics, CSTEP calculates the participation factors (**pf**), which provide the incidence of the system eigenvalues on the state variables and vice versa. These participation factors are calculated according to the following expression:

$$\mathbf{pf} = \mathbf{\Phi}^{\top} \odot \mathbf{\Psi} \tag{25}$$

where $\odot$ denotes the element-by-element or Hadamard product of the left and right eigenvectors of the state matrix $\mathbf{A}$. The tool also calculates the weighted participation factors (**wpf**) as in [15] to represent that incidence in a percentage or 0–1 scale:

$$\mathbf{wpf}\left(x_l, \lambda_j\right) = \frac{\left|\mathbf{pf}\left(x_l, \lambda_j\right)\right|}{\sum_{\mu}\left|\mathbf{pf}\left(\mu, \lambda_j\right)\right|} \tag{26}$$

where μ depicts the set of states for the eigenvalue λ_j.

4) Parametric sensitivity

CSTEP provides a couple of tools to estimate the influence of parameters on the system stability: a parametric sensitivity matrix (**ps**) and an iterative parametric sweep function. The so-called parametric sensitivities are calculated to study the movement of eigenvalues with respect to variations of any parameter of the system [24]. This matrix is obtained as follows:

$$ps_{jk} = \frac{\partial \lambda_j}{\partial \rho_k} = \frac{\mathbf{\Phi}_j^{\top} \dfrac{\partial \mathbf{A}}{\partial \rho_k} \mathbf{\Psi}_j}{\mathbf{\Phi}_j^{\top} \mathbf{\Psi}_j} \tag{27}$$

The use of symbolic notation in CSTEP makes it possible to calculate the exact sensitivity of each of the studied operation points.

5) Parametric sweeps

Parametric sweeps, on the other hand, can be carried out either using the symbolic or the numeric representation of the system. In the former, even though constructing the system model symbolically requires a higher computational effort than doing it numerically, the final symbolic expressions can be efficiently used afterwards to carry out iterative studies such as parametric sweeps without the need to reconstruct the linearized system matrices in Eq. (24) each iteration.

3. Validation and application of CSTEP

The aim of this section is threefold. Firstly, the purpose is to illustrate step-by-step how a very simple example is constructed and reduced with CSTEP (Use case I). Secondly, the tool is validated by comparing the time-domain response and eigenvalues of a 5-bus IEEE benchmark system to the same model developed in DigSilent PowerFactory (Use case II). Moreover, with this example, the incongruencies that might arise in terms of converter stability in both models for certain operating points due to the reduction of the electromechanical states are shown. Thirdly, the potential applications of CSTEP are demonstrated with a more complex CIGRÉ distribution system comprised of 14 buses (Use case III).

A. Use case I – Simple ac system

This benchmark is comprised of an ideal voltage source (Generator 1), an *RL* transmission line (Line 1), and an *RL* load (Load 1). The general diagram is illustrated in Figure 2a.

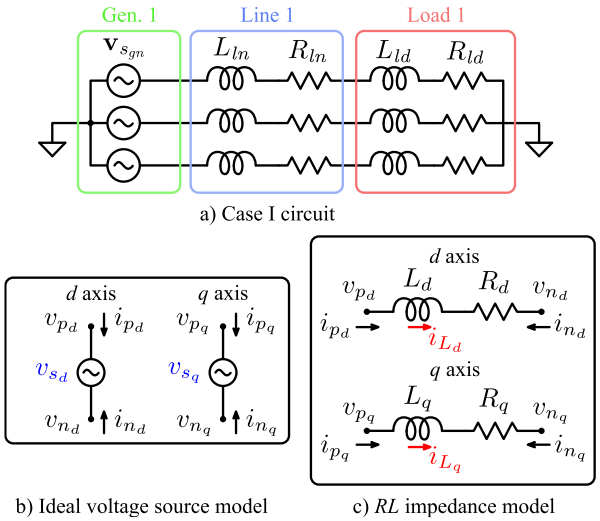

Figure 2 – Use case I: a) simplified ac system scenario, b) ideal voltage source library model, and c) *RL* impedance library model

In CSTEP, the ideal voltage source is modelled according to Figure 2b. The model has a *d* and *q* component, and there are no dynamic states. Since the element only has four node potential variables, it can be represented with the following four algebraic equations:

$$v_{s_d} = v_{p_d} - v_{n_d}; \quad v_{s_q} = v_{p_q} - v_{n_q}; \quad i_{p_d} = -i_{n_d}; \quad i_{p_q} = -i_{n_q} \tag{28}$$

where v_{s_d} and v_{s_q} are considered global inputs of the system.

Similarly, the line and load of the circuit can be modelled with the same *RL* library component (Figure 2c). In this case, there are two states associated with the inductances and four node potential variables, so the element of the *RL* impedance can be represented with the following set of differential-algebraic equations (DAE):

$$\begin{aligned}
\frac{di_{L_d}}{dt} &= \frac{1}{L_d}\left(v_{p_d} - R_d i_{L_d} - v_{n_d}\right) + \omega i_{L_q} \\
\frac{di_{L_q}}{dt} &= \frac{1}{L_q}\left(v_{p_q} - R_q i_{L_q} - v_{n_q}\right) - \omega i_{L_d} \\
i_{p_d} &= i_{L_d}; \quad i_{n_d} = -i_{L_d}; \quad i_{p_q} = i_{L_q}; \quad i_{n_q} = -i_{L_q}
\end{aligned} \tag{29}$$

where the coupling terms ωi_{L_q} and $-\omega i_{L_d}$ appear due to the conversion to the rotating *dq* reference frame. In this case, ω is considered a global input of the system.

1) Nonreduced system representation

Based on these library elements, the concatenated element equations (eqs. (5)–(8)) can be represented as follows:

$$\dot{\mathbf{x}}^S = \begin{bmatrix} \frac{di_{L_d}^{\mathrm{Ln}_1}}{dt} \\ \frac{di_{L_q}^{\mathrm{Ln}_1}}{dt} \\ \frac{di_{L_d}^{\mathrm{Ld}_1}}{dt} \\ \frac{di_{L_q}^{\mathrm{Ld}_1}}{dt} \end{bmatrix} = \begin{bmatrix} \frac{1}{L_d^{\mathrm{Ln}_1}}\left(v_{p_d}^{\mathrm{Ln}_1} - R_d^{\mathrm{Ln}_1} i_{L_d}^{\mathrm{Ln}_1} - v_{n_d}^{\mathrm{Ln}_1}\right) + \omega i_{L_q}^{\mathrm{Ln}_1} \\ \frac{1}{L_q^{\mathrm{Ln}_1}}\left(v_{p_q}^{\mathrm{Ln}_1} - R_q^{\mathrm{Ln}_1} i_{L_q}^{\mathrm{Ln}_1} - v_{n_q}^{\mathrm{Ln}_1}\right) - \omega i_{L_d}^{\mathrm{Ln}_1} \\ \frac{1}{L_d^{\mathrm{Ld}_1}}\left(v_{p_d}^{\mathrm{Ld}_1} - R_d^{\mathrm{Ld}_1} i_{L_d}^{\mathrm{Ld}_1} - v_{n_d}^{\mathrm{Ld}_1}\right) + \omega i_{L_q}^{\mathrm{Ld}_1} \\ \frac{1}{L_q^{\mathrm{Ld}_1}}\left(v_{p_q}^{\mathrm{Ld}_1} - R_q^{\mathrm{Ld}_1} i_{L_q}^{\mathrm{Ld}_1} - v_{n_q}^{\mathrm{Ld}_1}\right) - \omega i_{L_d}^{\mathrm{Ld}_1} \end{bmatrix} \tag{30}$$

$$\mathbf{g}_2^S = \begin{bmatrix} v_{s_d}^{\mathrm{Gn}_1} = v_{p_d}^{\mathrm{Gn}_1} - v_{n_d}^{\mathrm{Gn}_1} \\ v_{s_q}^{\mathrm{Gn}_1} = v_{p_q}^{\mathrm{Gn}_1} - v_{n_q}^{\mathrm{Gn}_1} \\ i_{p_d}^{\mathrm{Gn}_1} = -i_{n_d}^{\mathrm{Gn}_1} \\ i_{p_q}^{\mathrm{Gn}_1} = -i_{n_q}^{\mathrm{Gn}_1} \\ i_{p_d}^{\mathrm{Ln}_1} = i_{L_d}^{\mathrm{Ln}_1} \\ i_{n_d}^{\mathrm{Ln}_1} = -i_{L_d}^{\mathrm{Ln}_1} \\ i_{p_q}^{\mathrm{Ln}_1} = i_{L_q}^{\mathrm{Ln}_1} \\ i_{n_q}^{\mathrm{Ln}_1} = -i_{L_q}^{\mathrm{Ln}_1} \\ i_{p_d}^{\mathrm{Ld}_1} = i_{L_d}^{\mathrm{Ld}_1} \\ i_{n_d}^{\mathrm{Ld}_1} = -i_{L_d}^{\mathrm{Ld}_1} \\ i_{p_q}^{\mathrm{Ld}_1} = i_{L_q}^{\mathrm{Ld}_1} \\ i_{n_q}^{\mathrm{Ld}_1} = -i_{L_q}^{\mathrm{Ld}_1} \end{bmatrix}; \quad \mathbf{g}_4^S = \begin{bmatrix} v_{p_d}^{\mathrm{Gn}_1} = np_1 \\ v_{p_q}^{\mathrm{Gn}_1} = np_2 \\ v_{n_d}^{\mathrm{Gn}_1} = np_0 \\ v_{n_q}^{\mathrm{Gn}_1} = np_0 \\ v_{p_d}^{\mathrm{Ln}_1} = np_1 \\ v_{n_d}^{\mathrm{Ln}_1} = np_3 \\ v_{p_q}^{\mathrm{Ln}_1} = np_2 \\ v_{n_q}^{\mathrm{Ln}_1} = np_4 \\ v_{p_d}^{\mathrm{Ld}_1} = np_3 \\ v_{n_d}^{\mathrm{Ld}_1} = np_0 \\ v_{p_q}^{\mathrm{Ld}_1} = np_4 \\ v_{n_q}^{\mathrm{Ld}_1} = np_0 \end{bmatrix} \tag{31}$$

$$\mathbf{g}_7^S = \begin{bmatrix} 0 = i_{p_d}^{\mathrm{Gn}_1} + i_{p_d}^{\mathrm{Ln}_1} \\ 0 = i_{p_q}^{\mathrm{Gn}_1} + i_{p_q}^{\mathrm{Ln}_1} \\ 0 = i_{n_d}^{\mathrm{Ln}_1} + i_{p_d}^{\mathrm{Ld}_1} \\ 0 = i_{n_q}^{\mathrm{Ln}_1} + i_{p_q}^{\mathrm{Ld}_1} \end{bmatrix}; \quad 0 = pn_0 \tag{32}$$

2) Reduced system representation

From Figure 2 it is evident that the current of the line and the load is the same, meaning that in Eq. (30) there are two linearly dependent (redundant) differential equations. By reducing these equations and substituting the algebraic equations from (31) and (32) the following system of equations is obtained:

$$\dot{\mathbf{x}}_r^S = \begin{bmatrix} \frac{di_{L_d}^{\mathrm{Ln}_1}}{dt} \\ \frac{di_{L_q}^{\mathrm{Ln}_1}}{dt} \end{bmatrix} = \begin{bmatrix} \frac{v_{s_d}^{\mathrm{Gn}_1} - \left(R_d^{\mathrm{Ln}_1} + R_d^{\mathrm{Ld}_1}\right) i_{L_d}^{\mathrm{Ln}_1}}{L_d^{\mathrm{Ln}_1} + L_d^{\mathrm{Ld}_1}} + \omega i_{L_q}^{\mathrm{Ln}_1} \\ \frac{v_{s_q}^{\mathrm{Gn}_1} - \left(R_q^{\mathrm{Ln}_1} + R_q^{\mathrm{Ld}_1}\right) i_{L_q}^{\mathrm{Ln}_1}}{L_q^{\mathrm{Ln}_1} + L_q^{\mathrm{Ld}_1}} - \omega i_{L_d}^{\mathrm{Ln}_1} \end{bmatrix} \tag{33}$$

This system is therefore comprised of two state variables and three inputs:

$$\mathbf{x}_r^S = \begin{bmatrix} i_{L_d}^{\mathrm{Ln}_1} & i_{L_q}^{\mathrm{Ln}_1} \end{bmatrix}^\top ; \quad \mathbf{u} = \begin{bmatrix} v_{s_d}^{\mathrm{Gn}_1} & v_{s_q}^{\mathrm{Gn}_1} & \omega \end{bmatrix}^\top \tag{34}$$

where $i_{L_d}^{\mathrm{Ln}_1} = i_{L_d}^{\mathrm{Ld}_1}$ and $i_{L_q}^{\mathrm{Ln}_1} = i_{L_q}^{\mathrm{Ld}_1}$ are the reduced dependent state variables.

3) Linear system representation

From Eq. (33) it is noticeable that the system appears to be nonlinear, due to the multiplication between the inductor current and the reference frame rotation frequency (ω). The reason is that ω is defined as an input of the system, so that frequency variations can be performed if necessary. If this frequency was considered to be constant, the system in Eq. (33) would be linear and would not need any linearization. Following the process in Appendix A, by partially differentiating the equations in Eq. (33) with respect to (34), the linearized representation of the system can be obtained:

$$\begin{aligned} \mathbf{A} &= \begin{bmatrix} \frac{-\left(R_d^{\mathrm{Ln}_1} + R_d^{\mathrm{Ld}_1}\right)}{L_d^{\mathrm{Ln}_1} + L_d^{\mathrm{Ld}_1}} & \bar{\omega} \\ -\bar{\omega} & \frac{-\left(R_q^{\mathrm{Ln}_1} + R_q^{\mathrm{Ld}_1}\right)}{L_q^{\mathrm{Ln}_1} + L_q^{\mathrm{Ld}_1}} \end{bmatrix} \\ \mathbf{B} &= \begin{bmatrix} \frac{1}{L_d^{\mathrm{Ln}_1} + L_d^{\mathrm{Ld}_1}} & 0 & \frac{L_d^{\mathrm{Ln}_1} \bar{i}_{L_q}^{\mathrm{Ln}_1} + L_d^{\mathrm{Ld}_1} \bar{i}_{L_q}^{\mathrm{Ld}_1}}{L_d^{\mathrm{Ln}_1} + L_d^{\mathrm{Ld}_1}} \\ 0 & \frac{1}{L_q^{\mathrm{Ln}_1} + L_q^{\mathrm{Ld}_1}} & -\frac{L_q^{\mathrm{Ln}_1} \bar{i}_{L_d}^{\mathrm{Ln}_1} + L_q^{\mathrm{Ld}_1} \bar{i}_{L_d}^{\mathrm{Ld}_1}}{L_q^{\mathrm{Ln}_1} + L_q^{\mathrm{Ld}_1}} \end{bmatrix} \end{aligned} \tag{35}$$

where the upper bar denotes the steady-state value obtained by setting the derivative terms in Eq. (33) to zero (i.e., $\dot{\mathbf{x}}_r^S = 0$) and by solving the remaining system of algebraic equations.

4) Validation of the linearized state-space model

To ensure that the linearized system is representative of the original nonlinear system, a time-domain simulation is carried out with CSTEP, and the response of both systems with a voltage variation in the voltage source is compared. The initial parameters of the simulation are given in Table 1:

Table 1 – Parameters of Case I

Param.	Value	Param.	Value	Param.	Value
$v_{s_d}^{\mathrm{Gn}_1}$	100 V	$L_d^{\mathrm{Ln}_1}$	0.1 mH	$R_d^{\mathrm{Ln}_1}$	0.1 Ω
$v_{s_q}^{\mathrm{Gn}_1}$	0 V	$L_q^{\mathrm{Ln}_1}$	0.1 mH	$R_q^{\mathrm{Ln}_1}$	0.1 Ω
ω	100π rad/s	$L_d^{\mathrm{Ld}_1}$	30 mH	$R_d^{\mathrm{Ld}_1}$	20 Ω
		$L_q^{\mathrm{Ld}_1}$	30 mH	$R_q^{\mathrm{Ld}_1}$	20 Ω

The time-domain evolution of the states of the system (the current in this case) for a 0.1 p.u. *d*-axis voltage variation can be observed in Figure 3:

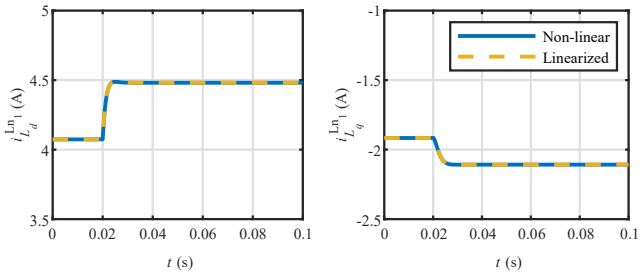

Figure 3 – Time-domain evolution of the system states in Case I for a 0.1 p.u. voltage variation

The results show that the linearized model is correctly representing the time-domain behaviour of the system even when moving out of the point at which the linearization is made. This means that the matrices in Eq. (35) can be employed to carry out a detailed modal analysis.

5) Modal analysis

The system has two eigenvalues and their properties have been gathered in Table 2:

Table 2 – Eigenvalues of Case I and their properties

Eigenvalue λ_j	**Damping** ζ_j	**Osc. Freq.** f_{o_j}	**Nat. Freq.** f_{n_j}
-667.77 + 314.16i	0.9	50 Hz	117.45 Hz
-667.77 - 314.16i	0.9	50 Hz	117.45 Hz

The oscillation frequency is the same as the reference frame rotation frequency, and the high damping values explain the overdamped response observed in Figure 3. The following two tables show the weighted participation factors (**wpf**) and the real part of the parametric sensitivity ($\Re\{\mathbf{ps}\}$ or **rps**) of the two eigenvalues.

wpf	λ_j	
x_l	0.5	0.5
	0.5	0.5

rps	$R_d^{\mathrm{Ln}_1}$	$R_q^{\mathrm{Ln}_1}$	$L_d^{\mathrm{Ln}_1}$	$L_q^{\mathrm{Ln}_1}$	$R_d^{\mathrm{Ld}_1}$	$R_q^{\mathrm{Ld}_1}$	$L_d^{\mathrm{Ld}_1}$	$L_q^{\mathrm{Ld}_1}$
x_l	-16.6	-16.6	1.1e4	1.1e4	-16.6	-16.6	1.1e4	1.1e4
	-16.6	-16.6	1.1e4	1.1e4	-16.6	-16.6	1.1e4	1.1e4

The participation factors show that the eigenvalues and the states are equally related, whereas the parametric sensitivity demonstrates that the inductances are the parameters that mostly influence the movement of eigenvalues in the complex plane. This can be also corroborated by carrying out a parametric sweep of the load resistance and inductance (see Figure 4). A small variation of the inductance causes the poles to move significantly in the real axis compared to higher variations in the resistance.

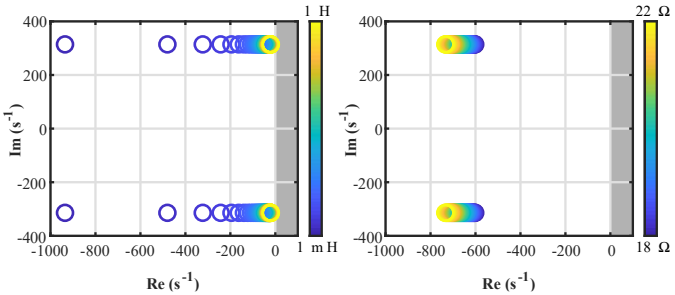

Figure 4 – Parametric sweep in Use case I: a) load inductance (from 1 mH to 1 H) and b) load resistance (from 18 Ω to 22 Ω).

B. *Use case II – IEEE 5-bus benchmark system*

The single line diagram of this use case is illustrated in Figure 5, where the green boxes represent the sources (in this case electronic converters), and the red triangles represent the loads. The values of the line impedances and the passive loads are indicated in the Figure. The employed voltage and power base values are 138 kV and 100 MVA, respectively.

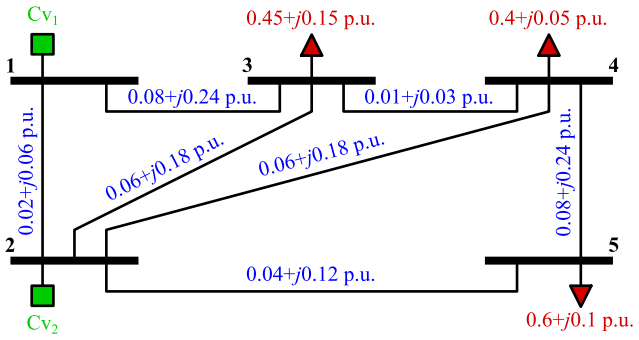

Figure 5 – IEEE 5-bus benchmark system (Use case II)

The converters are responsible for controlling the frequency of the grid by means of a grid-forming control strategy (Figure 6). In this case, the active power controller consists of a low-pass filter (equivalent to a virtual inertia) and a *p/f* droop regulator with gain K_p. The reactive power controller also includes a low-pass filter and a *q/v* droop regulator (K_q).

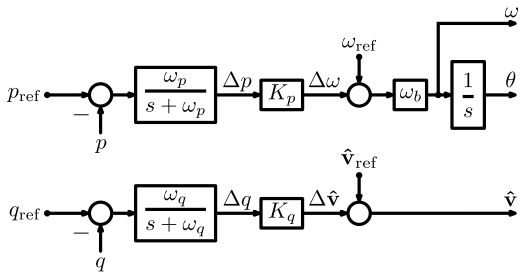

Figure 6 – Grid-forming control

The voltage amplitude and angle of the grid-forming control are used to obtain the converter reference voltage ($\mathbf{v}_{cv}^{*}$). The dc bus voltage of converters is assumed to be constant, and the switching operation is neglected by considering an average model of the converter as in [20,24]. This way, the converter output voltage ($\mathbf{v}_{cv}$) is decoupled from dc bus oscillations so that $\mathbf{v}_{cv} \approx \mathbf{v}_{cv}^{*}$. Moreover, an *LC* filter is included in the output of converters.

This use case has been constructed in CSTEP as well as in PowerFactory. Figure 7 represents the eigenvalues and the time-domain response of the system for a variation of 0.1 p.u. in the resistive part of the load connected to node 5. In the case of PowerFactory, the results obtained from the RMS model are represented, since the eigenvalues of the system cannot be obtained from the EMT model to carry out the small-signal stability analysis.

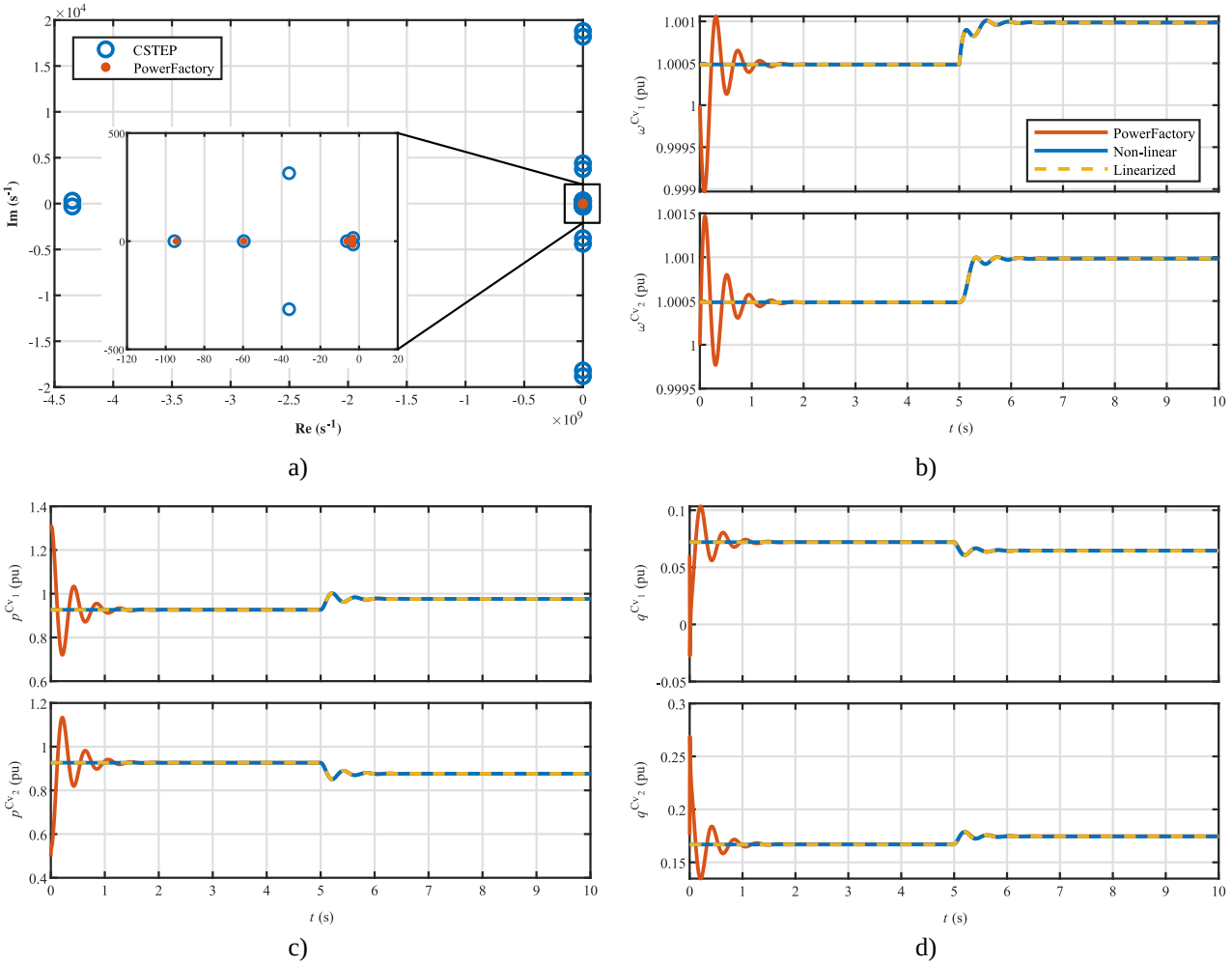

Figure 7 – Results of the IEEE 5-bus benchmark system: a) eigenvalues, b) converter control frequencies, c) converter active powers, d) converter reactive powers

In Figure 7a, it is observed that the eigenvalues represented by PowerFactory match correctly with the eigenvalues associated with the slowest states—i.e., with the lowest frequency—obtained with CSTEP. The reason for having such slow eigenvalues with converters is that the controllers are aimed at emulating the behavior of classical generators. In addition, CSTEP provides the eigenvalues associated with the faster electromagnetic states of the system. If the small-signal stability is assessed with the results from both tools, it can be concluded that the system is stable, but it can also be noted that the dominant eigenvalues (i.e., with less damping) differ significantly in both cases. In classical power systems where electromagnetic modes do not interact with fast-acting converters—e.g., when they are dominated by synchronous generators—the oscillations they cause are damped rapidly, and therefore such modes can be neglected.

This can be observed for instance in the results from the time-domain simulation in Figure 7b-d, where the evolution of converter frequencies and their active and reactive power are illustrated, respectively. Apart from the initial transient caused by the differences in the initial operating point in PowerFactory, the time-domain results show a very good match not only in steady-state, but also in the transient response after a load disturbance. Moreover, the nonlinear and the linearized models obtained in CSTEP also exhibit a good matching. These results validate the correctness of the core modules of CSTEP and mean that the conclusions obtained from the small-signal stability assessment are valid near the chosen equilibrium point.

One of the main contributions of CSTEP compared to already available tools arises when the controllers of electronic converters start interacting with faster states associated with the electric part of the grid, causing the eigenvalues to approach the unstable area. To illustrate this case, the reactive power droop gain from one of the converters in the 5-bus use case is modified, causing the dominant eigenvalues to move to the unstable area for certain points of operation (Figure 8a).

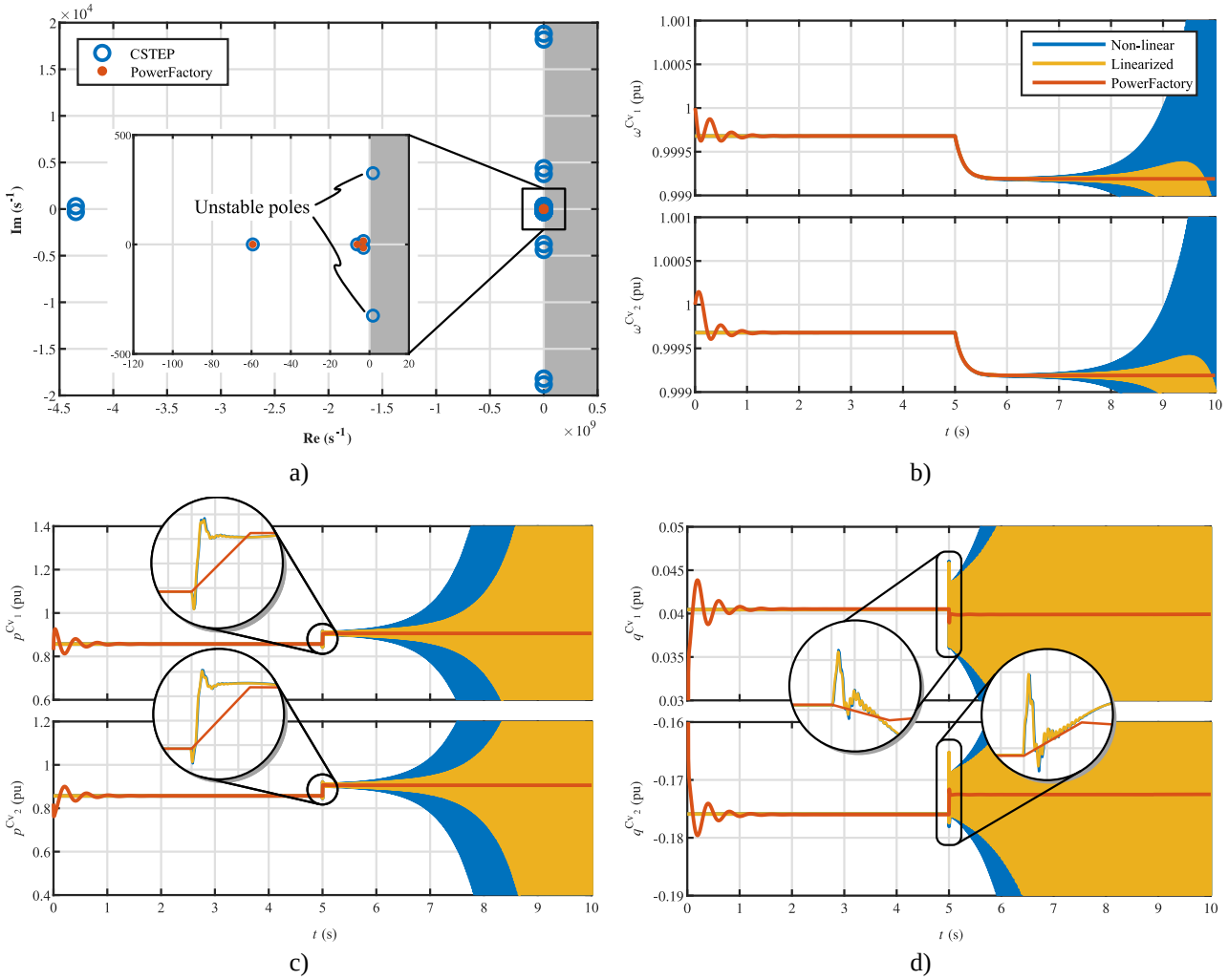

Figure 8 – Results of the IEEE 5-bus benchmark system for an unstable point of operation: a) eigenvalues, b) converter control frequencies, c) converter active powers, d) converter reactive powers

As it can be observed, the eigenvalues obtained from the RMS model in PowerFactory still coincide with the slower modes in CSTEP. However, in this case, PowerFactory does not consider the two dominant eigenvalues that make the system unstable, thus providing an incorrect conclusion in the assessment of the small-signal stability. This can be further

corroborated by looking at the time-domain response of the system in both tools (Figure 8b-d). The simulation is started from a stable point of operation, where CSTEP and PowerFactory provide almost the same results. At the instant t = 5s the disturbance in the load causes the system poles to cross to the unstable area, causing the time-domain response to approach infinity. However, the RMS model in PowerFactory from which eigenvalues are obtained converges to a new stable operating point. The differences of the modes considered in CSTEP and PowerFactory can be also observed in the transient after the disturbance at t = 5s; the enlarged sections in Figure 8c-d show the transient with different frequency components obtained in CSTEP, compared to the few points provided by the RMS model. Although this transient and the instability could be represented with more detail via an EMT simulation in PowerFactory, there is no option to calculate the eigenvalues from PowerFactory EMT model.

C. Use case III – CIGRÉ distribution system

The purpose of this use case is to illustrate the potential applications of CSTEP with a more complex use case. The scenario is based on the medium-voltage distribution network proposed by the CIGRÉ Task Force C6.04.02 in [25]. The topology is comprised of two feeders and 14 buses, as illustrated in Figure 9.

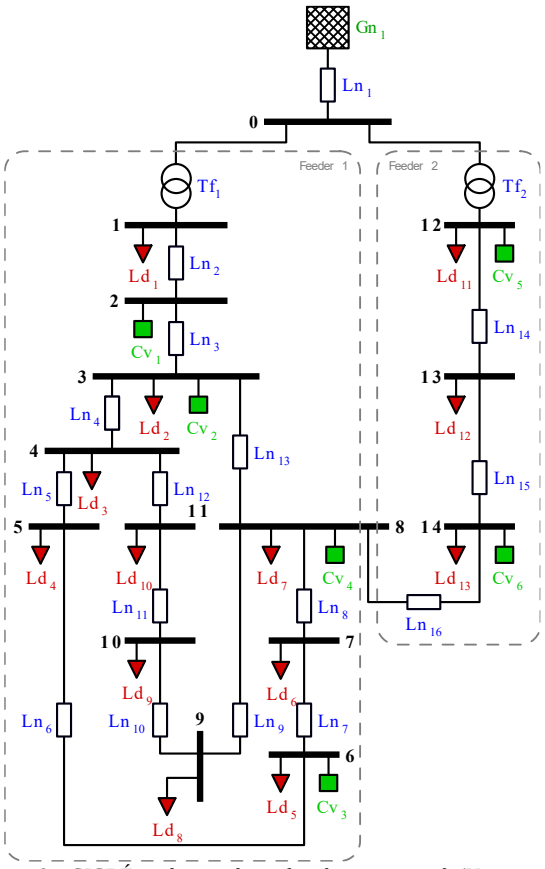

Figure 9 – CIGRÉ medium-voltage distribution network (Use case II)

The transformers and loads are modelled as equivalent *RL* impedances. On the other hand, transmission lines are modelled with two different fidelity levels to observe their effect on the small-signal stability. One benchmark variant is

modelled with *RL* transmission lines (named Variant 1), whereas the second one is modelled with nominal π transmission line circuits (Variant 2). The parameters of the transmission lines and transformers, as well as the generated/demanded power values, have been gathered from [25].

The use of simple element models for the considered test cases is justified since the objective of the paper is to illustrate the operation and functionalities of the tool rather than analysing the accuracy of the obtained results. On the other hand, converter-driven stability is closely linked to distributed generation, and thus to distribution lines. When the frequency spectrum of the signals involved is not too wide, and assuming frequency-independent line parameters, distribution lines are commonly represented in literature as cascaded π circuits. However, this approach has been also analysed for frequency-dependent transmission lines with satisfactory results in [26,27].

In Variant 1 there are 62 state variables, whereas in Variant 2 there are 122. These are automatically reduced by CSTEP to a representation of 34 and 88 state variables, respectively. The reason for this significant reduction is that many currents of the system depend on other ones (e.g., the current from loads depends on the line current), and that the capacitors of adjacent π equivalent transmission lines are connected in parallel (meaning that their voltage is equal). In other tools, the construction of such state-space models would have to be done either by manually writing all the equations (grouping adjacent inductors and capacitors) or by alternatively cascading π and *T* line models to avoid redundant states in the first place. Another alternative is the addition of "phantom" components to avoid the appearance of redundant states [19], but these parasitic elements introduce undesired dynamics and fictitious poles in the complex plane.

The root loci of the two benchmarks are illustrated in Figure 10. The right side of the figure shows that both systems exhibit some relatively damped modes at similar locations in the complex plane. These are primarily related to the inductances of the lines and loads. In addition to these, the left side of Figure 10 shows that Variant 2 exhibits several eigenvalues with an extremely low damping factor. In this case, their high imaginary component is caused by the low capacitance of the π equivalent transmission lines. Such low damping factors will cause high-frequency oscillations under power disturbances in the system.

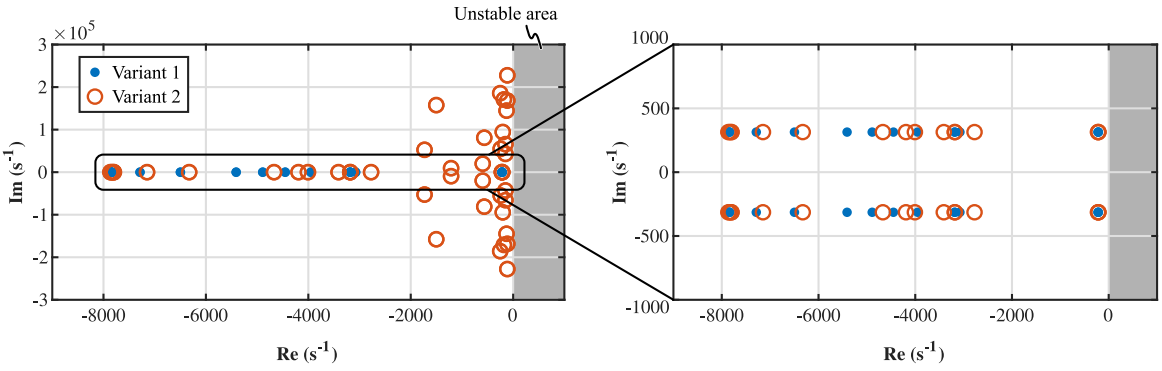

Figure 10 – Use case II: root loci of the CIGRÉ benchmark for *RL* transmission lines and π equivalent lines

The participation factor analysis of the eigenvalues shows that the most poorly damped eigenvalues—the so-called dominant modes—are associated with the state variables of transmission lines 2, 13 and 16 in Variant 1, and to 7, and 11 and 12 in Variant 2. This means that the buses adjacent to these lines are more prone to oscillate under the same load or generation variation. The frequency of these oscillations will be the same as the frequency of the eigenvalues, but the amplitude will be dependent on how these modes are excited. From this study, it can be already seen that the fidelity of transmission lines returns different dominant oscillation modes for the same benchmark.

Since another potential application of CSTEP is the study of the integration of converters in the grid, 6 converter-interfaced devices have been included in Variants 1 and 2 of Use case III. These converters are connected to the grid by means of *LC* filters and their location is shown in Figure 9. Their control consists of a classical power controller based on *dq* current PI regulators. The converters are equipped with a synchronous reference frame PLL (SRF-PLL) to synchronize with the grid.

The root loci of Variants 1 and 2 including these converters are shown in Figure 11. Apart from increasing the number of oscillatory modes, on the right side of the figure, it can be observed that the converters generate less damped oscillation modes compared to the previous results. This might lead to a more oscillatory behaviour under power disturbances. To study the effect of these additional modes, the simulation module provided by CSTEP is used.

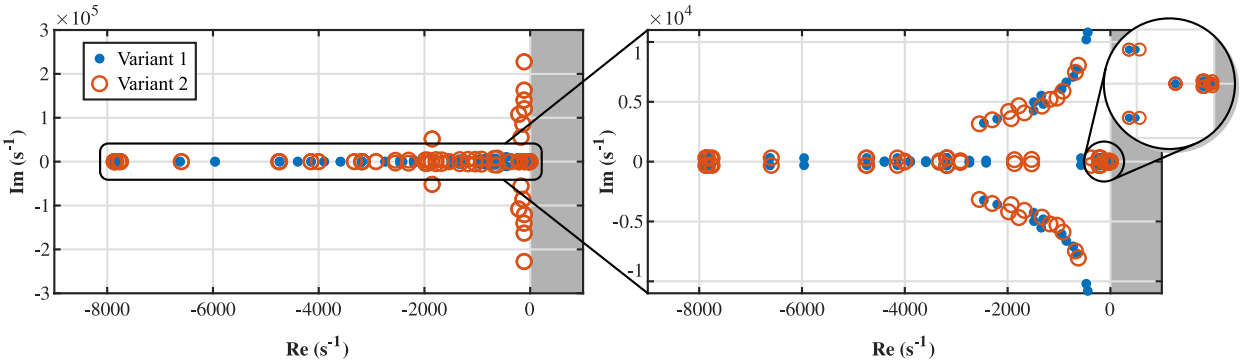

Figure 11 – Use case II: root loci of the CIGRÉ benchmark for the penetration of electronic power converters

Figure 12 shows the dynamic response of the current through line 1 for a 0.05 p.u. and a -0.1 p.u. power reference variation of Cv_3 at instants t = 1s and 3s, respectively. The comparison between the linearized (LIN) and nonlinear (NL) representations of Variants 1 and 2 shows that the small-signal models are accurate even for a 0.1 p.u. disturbance.

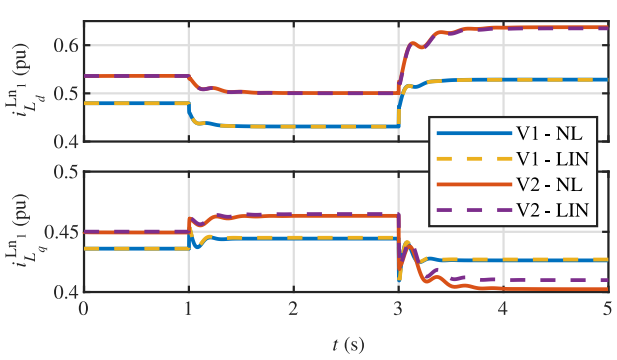

Figure 12 – Use case II: line 1 current evolution under 0.05 p.u. and -0.1 p.u. current perturbation of the inverter at instants t = 1s and 3s

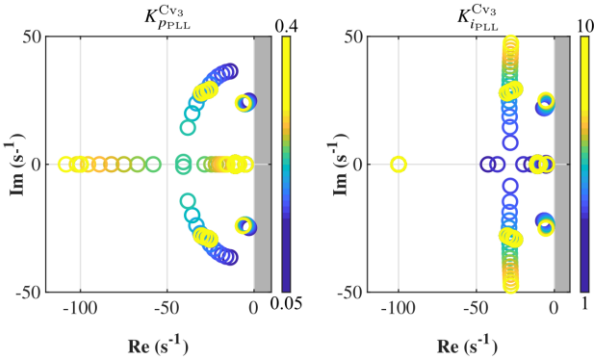

Figure 13 – Use case II-Variant 2: parametric sweep of PLL proportional and integral gains

Depending on the type of model employed for transmission lines, the system exhibits a different transient response under the same power disturbance, and the currents converge to different operation points in steady-state. In fact, Variant 2 exhibits a more oscillatory current response, and the q-axis term has a larger transient response and current excursion after the perturbation at t = 3s.

Following the example of Use case I the analysis can be extended, for example, by studying the effect of varying controller parameters on the movement of eigenvalues. Figure 13 shows the movement of eigenvalues in the complex plane for variations of the proportional and integral gains of the PLL of Cv_3. For instance, a slight modification of the proportional gain can significantly change the damping and hence the stability margins of the system.

This brings out the necessity not only to automatically build small-signal models, but also to provide a time-domain study to corroborate the analytical results. This does not make the small-signal model invalid or useless, because it can still be used to identify which are the states and parameters associated to the unstable modes, modify the design of the system and increase the stability margins.

Regarding the integral gain, the damping of poles varies for different values of the parameter. However, in this case, they do not tend to approach the unstable region.

The results elucidate that the topology of the studied system, the fidelity with which the transmission lines are modelled, or control parameters play a key role in the dynamic behaviour of the system. Other aspects such as the type of control employed at the converters, the model fidelity of transformers, or the consideration of a nonstiff grid in the system will also modify the dynamic properties of the system. However, since the purpose of this paper is to show the potential applications and advantages offered by CSTEP, these studies are left for future research activities.

CSTEP is providing information that might be challenging to get otherwise, since most available tools either 1) do not provide an automatic method for connecting element models, 2) do not consider the dynamics of line impedance, filters and converter controllers in the assessment of converter stability, and/or 3) they simulate the electromagnetic transients with a high level of detail for a short period but do not provide any analysis of the oscillation modes.

4. Conclusions

Power systems are suffering one of the most significant paradigm shifts because of the massive integration of electronic power converters. Even though there are a wide number of tools capable of carrying out stability analyses of conventional power systems, these tools do not consider the faster dynamics introduced by the electrical part of the grid or by power converters. This paper has described a new converter stability analysis tool called CSTEP to simulate and analyse the stability of power systems with a considerable penetration of converters. This tool makes it possible to consider not only the electromechanical dynamics of machines, but also the electromagnetic dynamics of the grid and the effect of converter topology and controllers.

In the paper, the mathematical foundations of the tool that enable to automatically construct and reduce the system of equations representing a specific use case have been introduced, based on the individual element models. Moreover, the time-domain simulation module and the analysis module of CSTEP have been described. The former is useful to simulate the original nonlinear representation and the linearized small-signal model of the system, which facilitates the validation of the linearized models for further analyses and provides information under large disturbances. The tool also incorporates several analysis techniques to study the stability margins of the system and to identify the influence of parameters on the dynamic behaviour of the system. Among these techniques, with CSTEP, it is possible to obtain the participation factors and the weighted participation factors that relate to the states and eigenvalues of the system, and the parametric sensitivities to estimate the effect of parameter variations in the location of eigenvalues. Moreover, it is possible to automatically perform parameter value sweeps to investigate their effect on the location of eigenvalues.

The system-building module algorithm has been demonstrated by means of a simplified ac use case, and the functionalities and potential applications of CSTEP have been highlighted using a converter-dominated 5-bus IEEE benchmark and the CIGRÉ medium voltage distribution grid as an example.

Acknowledgements

This work has been partially funded by the Spanish Ministry of Science and Innovation under the grant MTM2017-92996-C2-2-R and by the European Union's Horizon 2020 research and innovation program under grant agreement No. 963527 (iSTORMY—Interoperable, modular and Smart hybrid energy STORage system for stationary applications).

Appendix

A. Taylor series expansion

According to the Taylor series expansion, an arbitrary function $f(x)$ can be expanded around the equilibrium point $\bar{x}$ as:

$$f(x) = f(\bar{x}) + \left.\frac{df}{dx}\right|_{x=\bar{x}} (x-\bar{x}) + \frac{1}{2!}\left.\frac{d^2 f}{dx^2}\right|_{x=\bar{x}} (x-\bar{x})^2 + \frac{1}{3!}\left.\frac{d^3 f}{dx^3}\right|_{x=\bar{x}} (x-\bar{x})^3 + \cdots \tag{36}$$

When x is near $\bar{x}$, second and higher-order terms are very close to zero and therefore they can be neglected, obtaining the following approximation:

$$f(x) \approx f(\bar{x}) + \left.\frac{df}{dx}\right|_{x=\bar{x}} (x-\bar{x}) \tag{37}$$

By defining the variation of the state as $\Delta x = x - \bar{x}$, Eq. (37) can be rewritten as:

$$\Delta \dot{x} \approx \left.\frac{df}{dx}\right|_{x=\bar{x}} \Delta x \tag{38}$$

In a power system, equations depend not only on states but also on algebraic variables and inputs. Eq. (38) can be generalized to consider the effect of algebraic and input variables as:

$$\Delta \dot{x}_i \approx \sum_{l=1}^{m} \left.\frac{\partial f_i}{\partial x_l}\right|_{x_l=\bar{x}_l} \Delta x_l + \sum_{l=1}^{n} \left.\frac{\partial f_i}{\partial z_j}\right|_{z_l=\bar{z}_l} \Delta z_l + \sum_{l=1}^{o} \left.\frac{\partial f_i}{\partial u_l}\right|_{u_l=\bar{u}_l} \Delta u_l \tag{39}$$

where $\bar{x}$, $\bar{z}$ and $\bar{u}$ are the values of the states, algebraic variables, and inputs at the equilibrium point, respectively. These values are calculated by setting all the derivatives equal to zero (meaning the system is in steady-state) and solving the system of equations for x, z and u. The indices m, n and o represent the number of states, algebraic variables, and inputs, respectively. The matrices that group the partial derivatives of all system equations obtained according to Eq. (39) are known as Jacobian matrices, and they can be easily calculated by applying the *jacobian* command in MATLAB. The compact and grouped matrix form of the Jacobian matrices in Eq. (39) is shown in Eq. (17).

References

[1] F. Milano, F. Dorfler, G. Hug, D.J. Hill, G. Verbic, Foundations and Challenges of Low-Inertia Systems, in: 2018 Power Syst. Comput. Conf., IEEE, 2018: pp. 1–25. https://doi.org/10.23919/PSCC.2018.8450880.

[2] P. Kundur, J. Paserba, V. Ajjarapu, G. Andersson, A. Bose, C. Canizares, N. Hatziargyriou, D. Hill, A. Stankovic, C. Taylor, T. Van Cutsem, V. Vittal, Definition and Classification of Power System Stability IEEE/CIGRE Joint Task Force on Stability Terms and Definitions, IEEE Trans. Power Syst. 19 (2004) 1387–1401. https://doi.org/10.1109/TPWRS.2004.825981.

[3] Q. Peng, Q. Jiang, Y. Yang, T. Liu, H. Wang, F. Blaabjerg, On the Stability of Power Electronics-Dominated Systems: Challenges and Potential Solutions, IEEE Trans. Ind. Appl. 55 (2019) 7657–7670. https://doi.org/10.1109/TIA.2019.2936788.

[4] E. Unamuno, J.A. Suul, M. Molinas, J.A. Barrena, Comparative Eigenvalue Analysis of Synchronous Machine Emulations and Synchronous Machines, in: IECON 2019 - 45th Annu. Conf. IEEE Ind. Electron. Soc., IEEE, 2019: pp. 3863–3870. https://doi.org/10.1109/IECON.2019.8927826.

[5] M. Zhao, X. Yuan, J. Hu, Y. Yan, Voltage Dynamics of Current Control Time-Scale in a VSC-Connected Weak Grid, IEEE Trans. Power Syst. 31 (2016) 2925–2937. https://doi.org/10.1109/TPWRS.2015.2482605.

[6] N. Hatziargyriou, J. V. Milanovic, C. Rahmann, V. Ajjarapu, C. Canizares, I. Erlich, D. Hill, I. Hiskens, I. Kamwa, B. Pal, P. Pourbeik, J.J. Sanchez-Gasca, A.M. Stankovic, T. Van Cutsem, V. Vittal, C. Vournas, Definition and Classification of Power System Stability Revisited & Extended, IEEE Trans. Power Syst. (2020) 1–1. https://doi.org/10.1109/TPWRS.2020.3041774.

[7] M. Farrokhabadi, C.A. Canizares, J.W. Simpson-Porco, E. Nasr, L. Fan, P.A. Mendoza-Araya, R. Tonkoski, U. Tamrakar, N. Hatziargyriou, D. Lagos, R.W. Wies, M. Paolone, M. Liserre, L. Meegahapola, M. Kabalan, A.H. Hajimiragha, D. Peralta, M.A. Elizondo, K.P. Schneider, F.K. Tuffner, J. Reilly, Microgrid Stability Definitions, Analysis, and Examples, IEEE Trans. Power Syst. 35 (2020) 13–29. https://doi.org/10.1109/TPWRS.2019.2925703.

[8] X. Wang, F. Blaabjerg, Harmonic Stability in Power Electronic-Based Power Systems: Concept, Modeling, and Analysis, IEEE Trans. Smart Grid. 10 (2019) 2858–2870. https://doi.org/10.1109/TSG.2018.2812712.

[9] G. Gaba, S. Lefebvre, D. Mukhedkar, Comparative analysis and study of the dynamic stability of AC/DC systems, IEEE Trans. Power Syst. 3 (1988) 978–985. https://doi.org/10.1109/59.14550.

[10] E. Unamuno, A. Rygg, M. Amin, M. Molinas, J.A. Barrena, Impedance-Based Stability Evaluation of Virtual Synchronous Machine Implementations in Converter Controllers, in: 2018 Int. Power Electron. Conf. (IPEC-Niigata 2018 -ECCE Asia), IEEE, 2018: pp. 759–766. https://doi.org/10.23919/IPEC.2018.8507905.

[11] F. Milano, Á. Ortega Manjavacas, Frequency variations in power systems: Modeling, state estimation and control, Wiley-IEEE Press, 2020.

[12] J. Mahseredjian, V. Dinavahi, J.A. Martinez, Simulation Tools for Electromagnetic Transients in Power Systems: Overview and Challenges, IEEE

Trans. Power Deliv. 24 (2009) 1657–1669. https://doi.org/10.1109/TPWRD.2008.2008480.
[13] R.W. Kenyon, M. Bossart, M. Marković, K. Doubleday, R. Matsuda-Dunn, S. Mitova, S.A. Julien, E.T. Hale, B.-M. Hodge, Stability and control of power systems with high penetrations of inverter-based resources: An accessible review of current knowledge and open questions, Sol. Energy. 210 (2020) 149–168. https://doi.org/10.1016/j.solener.2020.05.053.
[14] C. Collados-Rodriguez, M. Cheah-Mane, E. Prieto-Araujo, O. Gomis-Bellmunt, Stability Analysis of Systems With High VSC Penetration: Where Is the Limit?, IEEE Trans. Power Deliv. 35 (2020) 2021–2031. https://doi.org/10.1109/TPWRD.2019.2959541.
[15] F. Shahnia, A. Arefi, Eigenanalysis-based small signal stability of the system of coupled sustainable microgrids, Int. J. Electr. Power Energy Syst. 91 (2017) 42–60. https://doi.org/10.1016/j.ijepes.2017.03.003.
[16] Z. Li, M. Shahidehpour, Small-Signal Modeling and Stability Analysis of Hybrid AC/DC Microgrids, IEEE Trans. Smart Grid. 10 (2019) 2080–2095. https://doi.org/10.1109/TSG.2017.2788042.
[17] D. Rimorov, J. Huang, C.F. Mugombozi, T. Roudier, I. Kamwa, Power Coupling for Transient Stability and Electromagnetic Transient Collaborative Simulation of Power Grids, IEEE Trans. Power Syst. 36 (2021) 5175–5184. https://doi.org/10.1109/TPWRS.2021.3075908.
[18] R. Venkatraman, S.K. Khaitan, V. Ajjarapu, Dynamic Co-Simulation Methods for Combined Transmission-Distribution System With Integration Time Step Impact on Convergence, IEEE Trans. Power Syst. 34 (2019) 1171–1181. https://doi.org/10.1109/TPWRS.2018.2874807.
[19] N. Watson, J. Arrillaga, Power Systems Electromagnetic Transients Simulation, IET, The Institution of Engineering and Technology, Michael Faraday House, Six Hills Way, Stevenage SG1 2AY, UK, 2003. https://doi.org/10.1049/PBPO039E.
[20] I. Caduff, U. Markovic, C. Roberts, G. Hug, E. Vrettos, Reduced-order modeling of inverter-based generation using hybrid singular perturbation, Electr. Power Syst. Res. 190 (2021) 106773. https://doi.org/10.1016/j.epsr.2020.106773.
[21] A.J. Agbemuko, J.L. Domínguez-García, O. Gomis-Bellmunt, Impedance-Based Modelling of Hybrid AC/DC Grids With Synchronous Generator for Interaction Study and Dynamic Improvement, Electr. Power Syst. Res. 179 (2020) 106086. https://doi.org/10.1016/j.epsr.2019.106086.
[22] P. De Rua, Ö.C. Sakinci, J. Beerten, Comparative Study of Dynamic Phasor and Harmonic State-Space Modeling for Small-Signal Stability Analysis, Electr. Power Syst. Res. 189 (2020) 106626. https://doi.org/10.1016/j.epsr.2020.106626.
[23] L.W. Nagel, SPICE2: A Computer Program to Simulate Semiconductor Circuits, 1975.
[24] S. D'Arco, J.A. Suul, O.B. Fosso, A Virtual Synchronous Machine implementation for distributed control of power converters in SmartGrids, Electr. Power Syst. Res. 122 (2015) 180–197. https://doi.org/10.1016/j.epsr.2015.01.001.
[25] K. Strunz, E. Abbasi, C. Abbey, C. Andrieu, U. Annakkage, S. Barsali, R.C. Campbell, R. Fletcher, F. Gao, T. Gaunt, A. Gole, N. Hatziargyriou, R. Iravani, G. Joos, H. Konishi, M. Kuschke, E. Lakervi, C.-C. Liu, J. Mahseredjian, F. Mosallat, D. Muthumuni, A. Orths, S. Papathanassiou, K. Rudion, Z. Styczynski, S.C. Verma, Benchmark Systems for Network Integration of Renewable and Distributed Energy Resources, 2014.
[26] J. Beerten, S. D'Arco, J.A. Suul, Identification and Small-Signal Analysis of Interaction Modes in VSC MTDC Systems, IEEE Trans. Power Deliv. 31 (2016) 888–897. https://doi.org/10.1109/TPWRD.2015.2467965.
[27] J.A.R. Macias, A.G. Exposito, A.B. Soler, A Comparison of Techniques for State-Space Transient Analysis of Transmission Lines, IEEE Trans. Power Deliv. 20 (2005) 894–903. https://doi.org/10.1109/TPWRD.2005.844271.